

Effect of pump-probe detuning on the Faraday rotation and ellipticity signals of mode-locked spins in InGaAs quantum dots

M. M. Glazov¹, I. A. Yugova², S. Spatzek³, A. Schwan³, S. Varwig³,
D. R. Yakovlev^{1,3}, D. Reuter⁴, A. D. Wieck⁴, and M. Bayer³

¹ *A. F. Ioffe Physical-Technical Institute, Russian Academy of Sciences, 194021 St. Petersburg, Russia*

² *Physical Faculty of St. Petersburg State University, 198504 St. Petersburg, Russia*

³ *Experimentelle Physik 2, Technische Universität Dortmund, D-44221 Dortmund, Germany and*

⁴ *Angewandte Festkörperphysik, Ruhr-Universität Bochum, D-44780 Bochum, Germany*

(Dated: August 26, 2010)

We have studied the Faraday rotation and ellipticity signals in ensembles of singly-charged (In,Ga)As/GaAs quantum dots by pump-probe spectroscopy. For degenerate pump and probe we observe that the Faraday rotation signal amplitude first grows with increasing the time separation between pump and probe before a decay is observed for large temporal separations. The temporal behavior of the ellipticity signal, on the other hand, is regular: its amplitude decays with the separation. By contrast, for detuned pump and probe the Faraday rotation and ellipticity signals both exhibit similar and conventional behavior. The experimental results are well described in the frame of a recently developed microscopic theory [Phys. Rev. B **80**, 104436 (2009)]. The comparison between calculations and experimental data allows us to provide insight into the spectral dependence of the electron spin precession frequencies and extract the electron g factor dependence on energy.

PACS numbers: 78.67.Hc, 78.47.-p, 71.35.-y

I. INTRODUCTION

Studies of electron spin dynamics in solids have recently become a rapidly developing field of condensed matter physics.^{1,2} Insight into the electron spin dynamics is provided by the pump-probe technique which has proven to be a versatile tool to address spin coherence.³ The basic idea behind this method is quite simple: the sample is illuminated by the circularly polarized pump pulse which creates a non-equilibrium spin orientation of charge carriers. After a certain time delay the weaker linearly polarized probe pulse hits the sample. The rotation of its polarization plane in transmission (spin Faraday effect) or in reflection (spin Kerr effect) geometry as well as the degree of its ellipticity serve as measures of the carrier spin polarization. Applied to semiconductor systems, the pump-probe technique allowed one to measure spin relaxation times, image electron spin diffusion, monitor spin precession caused by an external magnetic field and spin-orbit coupling, etc [see Refs. 1,4 and references therein].

The pump-probe technique has also turned out to be extremely useful to study the specifics of spin dynamics in n -type singly-charged semiconductor quantum dots (QDs) where long-lived spin coherence of resident electrons can be efficiently generated.⁵ The pump-probe method revealed the effects of spin mode-locking⁶ and of the coupled electron-nuclear spin dynamics.⁷

While the pump-probe technique is widely used experimentally, the microscopic processes responsible for Faraday/Kerr rotation and ellipticity signals were established for n -type QD systems only recently.⁴ In particular, it was demonstrated that, the Faraday rotation (FR) and ellipticity signals have strongly different spectral dependencies and, in case of a QD array, can provide information about different subensembles of electrons. The developed theory suggested that the temporal evolution of these signals can be quite different and depends strongly

on the energy detuning between the pump and probe pulses. Although in transverse magnetic field both ellipticity and Faraday rotation demonstrate oscillations resulting from the spin precession, for degenerate pump and probe pulses, the Faraday rotation signal amplitude may grow with an increase of the time separation between pump and probe pulses, contrary to the decay of the ellipticity signal. The observed spin beats frequencies are also different for the Faraday rotation and ellipticity signals.

This paper aims at illustrating experimentally the theoretical predictions of Ref. 4. We present experimental data on Faraday rotation and ellipticity signals in n -type (In,Ga)As/GaAs singly-charged QDs in the vicinity of the trion resonance, where the pump and probe energies have been varied relative to each other. This particular experimental configuration (i) enables us to monitor the spin dynamics of resident carriers, and (ii) allows a direct comparison with the theory of Ref. 4. We demonstrate good agreement of the experimental data with the theory.

In Section II we present an overview of the studied sample and the experimental techniques. The experimental results are summarized in Sec. III. Section IV discusses the theoretical background and presents the comparison of the experimental data with the model calculations. A brief summary of the results is given in Sec. V.

II. SAMPLE AND EXPERIMENTAL TECHNIQUE

The studied heterostructure was grown by molecular-beam epitaxy and consists of 20 layers of (In,Ga)As/GaAs QDs separated by 60 nm GaAs barriers with a QD density of about 10^{10} cm⁻² in each layer.^{6,8} The δ -sheets of Si donors were positioned at the distance of 20 nm below each QD layer with the dopant density being roughly equal to the dot density

in order to achieve an average occupation of a single electron per dot. The as-grown InAs/GaAs sample shows ground-state photoluminescence around 1.05 eV at cryogenic temperatures. It was thermally annealed for 30 seconds at 945°C to shift the emission energy to 1.398 eV due to Ga diffusion into InAs QDs.

In the experiments the spin coherence was measured by a time-resolved two-color pump-probe technique. Two pulsed Ti:Sapphire lasers acting as pump and probe were synchronized to each other at a repetition rate of 75.75 MHz corresponding to a repetition period of $T_R = 13.2$ ns. The pulse duration of both lasers was 2 ps, and their photon energies could be tuned independently. The power ratio of the lasers was about 5 (pump) to 1 (probe). The pump beam was modulated with a photoelastic modulator, changing between left- and right-handed circular polarizations at 50 kHz frequency. The probe beam was linearly polarized. The pump laser energy was tuned in resonance with the maximum of the photoluminescence of the QDs, $\hbar\omega_P = 1.398$ meV (see Refs. 5,6 for details), while the probe energy was varied relative to the pump one. We used a lock-in amplifier technique for time-resolved Faraday rotation and ellipticity measurements to monitor the spin coherence excited by the circularly polarized pump. The time delay between pump and probe was tuned by a mechanical delay line by which delays up to 6.6 ns with a precision of 7 fs could be scanned. After passage through the sample the probe beam was sent through a $\lambda/2$ (for Faraday rotation) or $\lambda/4$ (for ellipticity) plates and the intensities of the two contained orthogonal polarizations were measured by a balanced photodiode bridge.

The sample was mounted in a cryostat with a split-coil superconducting magnet and cooled down to a temperature $T = 6$ K. An external magnetic field was applied in the plane of the sample orthogonal to the light propagation direction (Voigt geometry). Its strength was chosen to be $B = 4$ T.

III. EXPERIMENTAL RESULTS

The important property of the QD samples under study, which is crucial for the FR and ellipticity signal formation, is their inhomogeneity. Indeed, photoluminescence reveals a broad (~ 10 meV) distribution of the singlet trion resonance frequencies in the sample.⁵ The pump pulse excites only a part of this distribution according to its spectral width of about 1 meV. The excited subensemble contains around a million QDs with different trion resonance frequencies, ω_0 , and different spin precession (Larmor) frequencies Ω_L . The interaction of a circularly polarized photon with a quantum dot electron is spin-dependent, and therefore can result in generation of spin coherence in the QD.⁵

The spin dynamics is probed by the weak linearly polarized probe pulse. The response to this pulse is also dominated by the trion formation: depending on the electron spin orientation one of the circular components of the linear pulse interacts with the quantum dot more efficiently than the other one. As a result the probe pulse

transmitted through the sample acquires a degree of ellipticity, and its polarization plane is rotated as compared with its initial orientation.

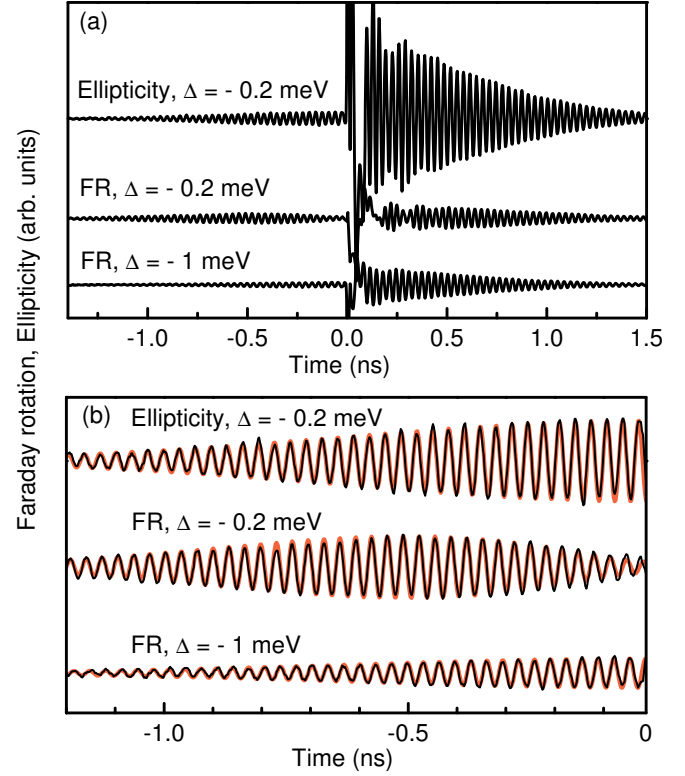


Figure 1: (Color online) (a) Time-resolved Faraday rotation and ellipticity signals. Top two curves show ellipticity and Faraday rotation signals for almost degenerate pump and probe ($\hbar\omega_P - \hbar\omega_{Pr} = \Delta = -0.2$ meV), bottom curve presents the Faraday rotation signal for detuned probe ($\Delta = -1.0$ meV). Panel (b) shows close-ups of the corresponding signals at negative time delay. Thin black curves are the experimental data, thick red curves are the results of fitting. $T = 6$ K, $B = 4$ T.

Experimental ellipticity and Faraday rotation signals as functions of the pump-probe time delay are presented in Fig. 1(a). The top two curves show signals for almost degenerate pump and probe. The small detuning between pump, $\hbar\omega_P$, and probe, $\hbar\omega_{Pr}$, energies, $\Delta = \hbar\omega_P - \hbar\omega_{Pr} = -0.2$ meV, was chosen to compensate a slight asymmetry of the photoexcited QD distribution and to make the features of the FR signal more pronounced, see below.⁹ The lowest curve shows FR signal for strongly detuned pump and probe ($\Delta = -1.0$ meV). Parts of these signals at negative delays are magnified in Fig. 1(b). The red curves in the figure show fits of the data according to

$$\mathcal{E}(t), \mathcal{F}(t) = \sum_i [\alpha_i \cos(\Omega_i |t| - \varphi_i) + \beta_i |t| \sin(\Omega_i |t| - \varphi_i)] \exp\left(-\frac{t^2}{2\tau_i^2}\right), \quad (1)$$

where $\mathcal{E}(t)$, $\mathcal{F}(t)$ are the ellipticity or FR signals as function of the delay t between the pump pulse and the subsequent probe pulse. The subscript i enumerates differ-

ent components in the experimental signal related with the spin dynamics of different carriers and their complexes, see below, α_i and β_i are the signal amplitudes, τ_i is the decay time and φ_i is the initial phase of the oscillatory components. The signals demonstrate oscillations resulting from the spin precession of electrons and holes about the in-plane magnetic field.^{5,8} The temporal dependence of the envelope function is qualitatively different for the FR and ellipticity signals in the (almost) degenerate pump-probe case. The envelope of the ellipticity signal decays with an increase of the time separation $|t|$, while the FR signal first grows with time separation before a decay is observed. This is especially well manifested at negative delays, see middle curve in Fig. 1(b). The increase of FR signal with time separation $|t|$ is an important feature of the experimental data observed at small pump-probe detunings $|\Delta| \lesssim 0.5$ meV.

For strongly detuned pump and probe the increase of FR rotation signal with pump-probe time separation is absent [lowest curve in Fig. 1(b)], and the FR signal becomes similar to the ellipticity one for the same detuning (not shown).

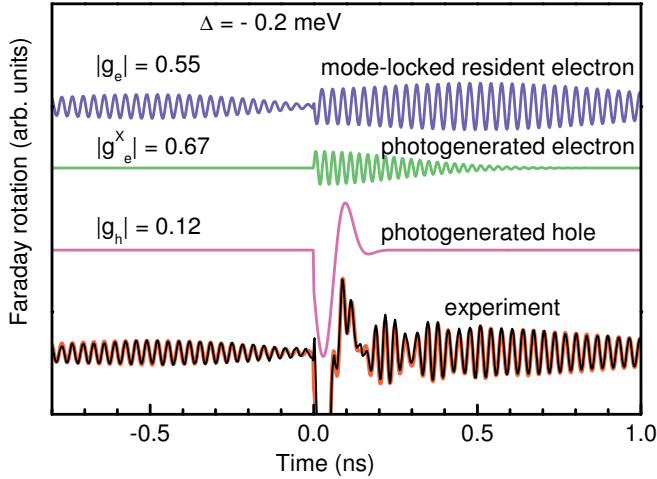


Figure 2: (Color online) Faraday rotation signal (lowest curves) for almost degenerate pump and probe pulses: experimental data shown by the black curve are superimposed on the fit (red curve). Three top dependencies are components to the fit (from top to bottom): signal due to long-lived electron spin polarization in charged QDs, signal due to the electron-in-exciton spin precession and signal due to hole-in-exciton spin precession in neutral QDs.⁸ $T = 6$ K, $B = 4$ T.

The complicated shape of the observed signals demonstrates that different physical processes are involved in the formation of the signals. In order to gain insight into the effects responsible for the signals and to isolate the contribution caused by the resident electrons we fitted the experimental data using Eq. (1). The different components contained in the experimental signal are demonstrated in Fig. 2. The lowest black curve represents the experimental data. It is superimposed on the red fit curve, which consists of three components that are shown separately at the top of Fig. 2. These three dependencies are labeled by the g factor values obtained from the spin beats frequency by $\hbar\Omega_L = g\mu_B B$, where Ω_L is the beats frequency and μ_B is the Bohr magneton.

Two of these three components appear only at positive delays. They are attributed to the spin precession of the hole ($|g_h| = 0.12$) and the electron forming the exciton in neutral QDs ($|g_e^X| = 0.67$). This conclusion is supported by the values of the g factors and the decay times being in agreement with Ref. 8. Note, that the effective g factor of the electron-in-exciton component $|g_e^X| = 0.67$ includes the contribution of the electron-hole exchange interaction, and therefore it differs from the resident electron g factor at the same transition energy.

The main part of the signal, shown by the top (blue) curve in Fig. 2, is due to the long-lived electron spin coherence in charged QDs: its lifetime exceeds by far the radiative lifetimes of excitons and trions in these quantum dots⁸ and the extracted g factor values are consistent with those of resident electrons with the same transition energy. The almost exact agreement between the fit and the experiment is demonstrated [red curve in the bottom of Fig. 2 determined using Eq. (1)] suggesting that all main contributions to the measured FR signal are taken into account.

The described fitting procedure was applied to all measured curves. Figure 3 displays the extracted long-lived electron spin coherence contributions for the ellipticity and FR signals presented Fig. 1(a). It is clearly seen that for the degenerate pump-probe conditions ($\Delta = -0.2$ meV) the FR signal increases with increasing pump-probe time separation, $|t|$. This behavior is in striking contrast to the ellipticity signal and the FR signal for detuned pump and probe.

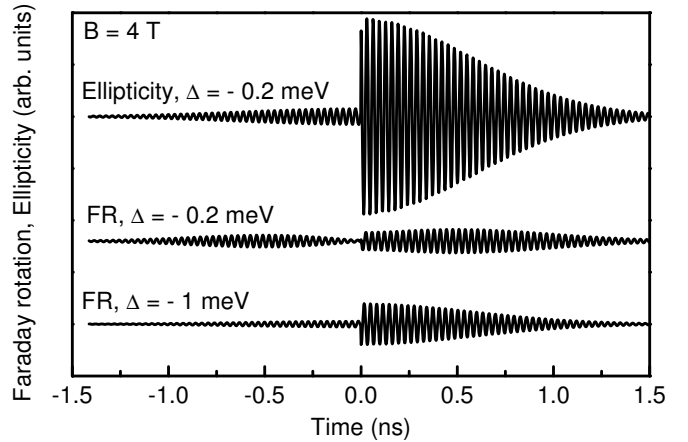


Figure 3: Long-lived parts of the Faraday rotation and ellipticity signals shown in Fig. 1(a) as extracted from the fit (shown in Fig. 2).

For an in-depth analysis we plot in Fig. 4 the amplitudes of the long-lived components of the ellipticity and FR signals extracted from the fit to the experimental data as functions of pump-probe detuning. For the ellipticity signal the contribution to the signal amplitude that is growing with pump-probe time separation $|t|$ is not observed, i.e. $\beta_{\text{neg}} = \beta_{\text{pos}} = 0$. Therefore, we plotted only the amplitudes α_{neg} for negative (circles) and α_{pos} for positive (squares) delays. For the FR signal both the decaying- and the growing-with-separation contributions are substantial: the amplitudes α of the decaying com-

ponent are shown in the main panel of Fig. 4(b), and the amplitudes β of the growing component are given in the inset for positive (squares) and negative (circles) time delays.

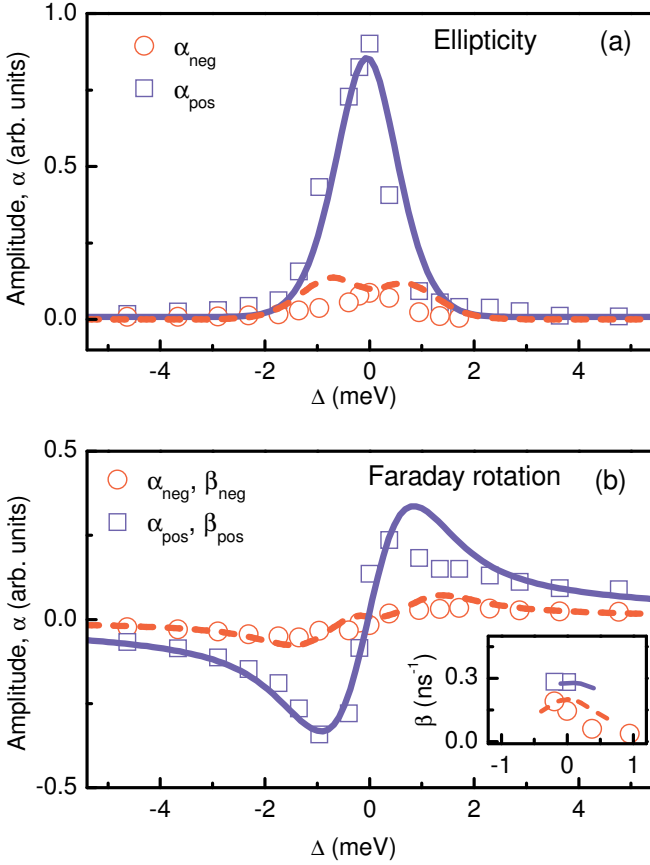


Figure 4: (Color online) Amplitudes of the ellipticity signal (a) and Faraday rotation signal (b) as function of pump-probe detuning. Circles show the amplitudes α_{neg} of the decaying component of the signal at negative delays and squares show the corresponding amplitudes α_{pos} at positive delays, see Eq. (1). Inset in panel (b): amplitudes of the growing component of the FR signal β_{neg} (circles) at negative delays and β_{pos} (squares) at positive delays. Lines are theoretical calculations in the frame of the model developed in Ref. [4], see Sec. IV.

One sees in Fig. 4(a) that the amplitude of the ellipticity signal is maximum for almost degenerate pump and probe, while the amplitude of the decaying part of the FR signal is (within the accuracy of the measurements⁹) an odd function of the detuning. Its absolute value reaches a maximum for pulses detuned by about 1 meV, see Fig. 4(b), in agreement with previous studies on quantum well¹⁰ and quantum dot^{11,12} samples. On the other hand, the component of the FR signal that is growing with time separation has not been observed in previous studies to the best of our knowledge. Its spectral behavior is opposite to that of the decaying part of the FR signal, as it reaches maximum for degenerate pump and probe and rapidly decreases with detuning, as shown in the inset of Fig. 4(b).

Finally, let us consider the dependence of the spin beats frequencies on the pump-probe detuning measured

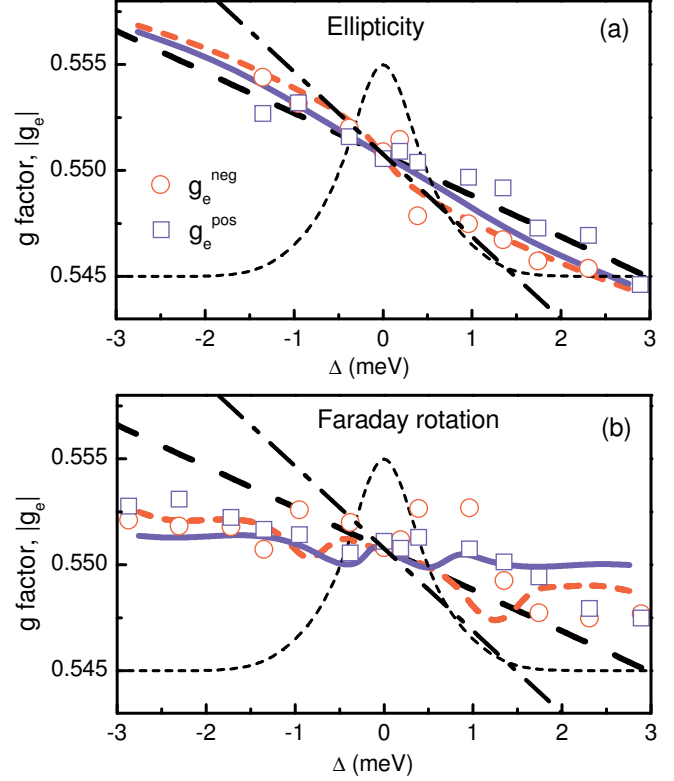


Figure 5: (Color online) Absolute values of electron g factors extracted from ellipticity signals (a) and Faraday rotation signals (b) as functions of pump-probe detuning. Circles and squares are experimental data obtained at negative and positive time delays, respectively. Dash-dotted line presents spectral dependence of electron g factor calculated after Eq. (2) with the constants $a = -0.004 \text{ meV}^{-1}$ and $c = 6.142$ taken from fitting the ellipticity by Eq. (7a) as function of Δ . Dashed line shows $|g_e|$ dependence calculated in the frame of a simple analytical model, Eq. (8). Red (dashed) and blue (solid) curves are the results of theoretical calculations (as described in Sec. IV C). Short dashed curve is integrated over the additional spread of Larmor frequencies, Ω_L, S_z^+ [see Eqs. (3) and (5)].

for the ellipticity and FR signals. It is well established that the electron g factor value and, correspondingly, the Larmor frequency have energy dispersion due to the effective band gap variation and, hence, they depend on the trion resonance (optical transition) frequency ω_0 .^{6,13,14} Over narrow energy ranges such a dependence can be well approximated by a linear function as⁴

$$|g_e(\omega_0)| = a\hbar\omega_0 + c, \quad (2)$$

with a and c being constants. Figure 5 shows the detuning dependencies of $|g_e|$ extracted from the ellipticity signal [panel (a)] and the Faraday rotation signal [panel (b)]. Circles show the values of g_e^{neg} , measured at negative delays and squares show the g -factors, g_e^{pos} , at positive delays. For the FR signal the g factors corresponding to the growing and decaying components are identical, therefore we plot only values corresponding to the decaying part of the signal.

A good correlation of the g -factor values obtained at positive and negative delays is seen. It indicates that

the same electron subensembles contribute to the signals at positive and negative delays. Although the g factors extracted from ellipticity and FR signals are quite close to each other, one can see from Fig. 5, that the spectral dependencies of g factor from the ellipticity signals have a different slope as those from the FR signals. The FR g factor data shown in panel (b) has a much weaker spectral dependence than the ellipticity data, shown in panel (a). Moreover, the spectral dependence of the g factor values extracted from ellipticity is weaker than the one predicted by Eq. (2), dash-dotted line in Fig. 5(a).

The main experimental findings can be summarized as follows:

- Faraday rotation and ellipticity signals measured for degenerate pump-probe conditions have drastically different temporal dependencies: the ellipticity signal amplitude decays with time separation between pump and probe, while the Faraday rotation signal contains, in addition to the decaying part, a growing component.
- For relatively large (as compared with the pump and probe pulse spectral widths) detunings the growing component of Faraday rotation signal disappears so that FR becomes similar to the ellipticity signal.
- The amplitude of the decaying component of ellipticity signal is an even function of the pump-probe detuning, while that of the Faraday rotation signal is an odd function.
- The dependencies of the electron g factor on probe spectral position, extracted from the ellipticity and Faraday rotation measurements, are different: the Faraday rotation g factor values demonstrate a weak spectral dependence in contrast to the ellipticity ones.
- The slope of the electron g -factor dependence on the probe spectral position is smaller than one in Eq. (2).

Below we present qualitative and quantitative discussion of these features.

IV. THEORY AND DISCUSSION

A. General considerations

In order to model the temporal dynamics of the Faraday rotation and ellipticity signals we follow the methods developed in Ref. 4. We consider an array of singly-charged n -type QDs subject to a train of circularly polarized pump pulses with the optical transition frequency ω_P . It is assumed that ω_P is close to the trion resonance frequency, ω_0 , therefore only one optical transition related with the formation of the singlet trion state is relevant. Depending on the initial spin orientation of the resident electron before pump pulse arrival, $\mathbf{S}^{(b)}$, trion formation is either possible or blocked due to the

Pauli principle for a given circular polarization of the pump pulse. As a result, electrons with a certain spin z -component, i.e. $-1/2$, take part in the trion formation for σ^+ circularly polarized light and they are left depolarized after trion recombination due to the fast hole spin relaxation^{4,15} (see also Ref. 10 for other regimes of electron spin coherence initialization). Therefore the electron spin before, $\mathbf{S}^{(b)}$, and after, $\mathbf{S}^{(a)}$, the pump pulse are correlated: there is an additive contribution which describes spin coherence generation by the pump pulse and a non-additive one which depends on (i) the pump pulse parameters and (ii) $\mathbf{S}^{(b)}$ and describes spin change by the pump pulse action.^{4,16,17} Explicit expressions for this action are presented by Eqs. (16) in Ref. 4.

Between the pump pulses the resident electron spins precess about the in-plane external field \mathbf{B} and decay due to spin relaxation processes. The latter can be characterized by a single time constant τ_s . Usually, τ_s exceeds by far the pulse repetition period, T_R , so that a steady state distribution of precessing spins is formed.^{4,6} We denote by $S_z^+(\omega_0; \omega_P)$ the electron spin z component in the steady state right after the arrival of the pump pulse in a QD with the trion resonance frequency ω_0 .

The time-resolved ellipticity $\mathcal{E}(t)$ and Faraday rotation $\mathcal{F}(t)$ signals measured by the probe with optical frequency ω_{pr} are given by the real and imaginary parts of the following convolution⁴

$$\mathcal{E}(t) + i\mathcal{F}(t) = \int p(\omega_0, \Omega_L) G(\omega_{pr} - \omega_0) S_z^+(\omega_0, \omega_P) \times \cos[\Omega_L t + \varphi(\omega_0, \Omega_L)] \exp(-t/\tau_s) d\omega_0 d\Omega_L. \quad (3)$$

Here the delay between the pump pulse and the next probe pulse $t > 0$. Function $p(\omega_0, \Omega_L)$ is the joint distribution function of optical and Larmor frequencies of QDs, and the function $G(\Lambda)$ characterizes the spectral sensitivity of the ellipticity and FR signals with Λ being the detuning between the probe carrier frequency and the QD trion resonance frequency. The last two factors in Eq. (3) describe the dynamics of a single spin in a given QD, which includes spin precession and spin relaxation. Here, $\varphi(\omega_0, \Omega_L)$ is the initial spin phase.^{4,15}

B. Illustrative example

It is the combined effect of the spectral variation of the function $G(\Lambda)$ and the dependence of the Larmor frequency on the optical frequency which determines the temporal evolution of the ellipticity and FR signals. In order to illustrate the qualitative behavior of these signals we employ a simple model, in which the function $G(\Lambda)$ is assumed to have the form

$$G(\Lambda) = (1 + 2i\Lambda\tau_p) \exp[-(\Lambda\tau_p)^2], \quad (4)$$

where τ_p is the pulse duration and $\Lambda = \omega_{pr} - \omega_0$ is the detuning between the probe pulse and the quantum dot trion resonance frequency. This function captures the main features of ellipticity and FR spectral sensitivity: the ellipticity has its maximum for $\Lambda = 0$, while the Faraday rotation is an odd function of the detuning, having

maxima of opposite signs on its wings. The form of $G(\Lambda)$ is approximate, nevertheless for $\Lambda\tau_p \lesssim 1$ the function $G(\Lambda)$ given by Eq. (4), is quite similar to the behavior of the exact spectral function for Rosen&Zener pulses, see Eq. (61) in Ref. 4. It is worth to mention that for $\Lambda\tau_p \gg 1$ the imaginary part of G (i.e. the FR sensitivity) decays faster than the exact function,¹⁸ but this does not affect the temporal behavior of the signals on a qualitative level.

For the distribution function of the optical and Larmor precession frequencies, $p(\omega_0, \Omega_L)$, we assume that: (i) the distribution of the optical frequencies is rather smooth, and (ii) there is a correlation between the electron g factor and the trion resonance frequency given by Eq. (2):

$$p(\omega_0, \Omega_L) = \frac{1}{\sqrt{2\pi}\Delta\Omega} \exp \left[-\frac{(\Omega_L - \mu_B g_e(\omega_0)B/\hbar)^2}{2(\Delta\Omega)^2} \right], \quad (5)$$

where $\Delta\Omega$ is the the spin precession frequency dispersion related, e.g., to nuclear field fluctuations. Finally, we assume that the steady state distribution of precessing spins is described by a Gaussian (the effects of mode-locking which result in the modification of S_z^+ for certain Larmor and optical frequencies⁴ are discussed below)

$$S_z^+(\omega_0, \omega_P) = S_0 \exp [-(\omega_0 - \omega_P)^2 \tau_p^2], \quad (6)$$

with S_0 being a constant, which depends on the pump amplitude.

Under these assumptions the convolutions in Eq. (3) can be easily evaluated.¹⁹ To simplify the analysis we disregard the fluctuations of the spin precession frequency, which are not correlated with the resonance frequency, i.e., put $\Delta\Omega = 0$ in Eq. (5) and additionally consider the limit of $\tau_s \rightarrow \infty$. Inclusion of these effects would simply enhance the decay of the spin beats. We also ignore the initial phase of the spin beats [i.e. we put $\varphi(\omega_0, \Omega_L) = 0$] because it does not bring in any new physics. The resulting signals are

$$\mathcal{E}(t) = \sqrt{\frac{\pi}{2\tau_p^2}} \exp \left[\frac{-\Delta^2 \tau_p^2 / (2\hbar^2) - (\Omega' t)^2}{8\tau_p^2} \right] \cos(\tilde{\Omega}_0 t), \quad (7a)$$

$$\mathcal{F}(t) = \frac{1}{2} \sqrt{\frac{\pi}{2\tau_p^2}} \exp \left[\frac{-\Delta^2 \tau_p^2 / (2\hbar^2) - (\Omega' t)^2}{8\tau_p^2} \right] \times \left[\frac{2\Delta\tau_p}{\hbar} \cos(\tilde{\Omega}_0 t) + \frac{\Omega' t}{\tau_p} \sin(\tilde{\Omega}_0 t) \right]. \quad (7b)$$

Here we introduced the following notations: $\Omega' = d\Omega_L/d\omega_0 = \mu_B a B$, $\Delta/\hbar = \omega_P - \omega_{pr}$ is the pump-probe detuning and $\tilde{\Omega}_0 = \Omega_0 + \Omega' \Delta / (2\hbar)$ is the effective spin precession frequency, with $\hbar\Omega_0 = g_e(\omega_{pr})\mu_B B$.

It follows from Eqs. (7a) and (7b) that the temporal behavior of the FR and ellipticity signals can be strongly different. This is especially well seen for degenerate pump and probe where the amplitude of the FR signal first grows with pump-probe time separation and afterwards decays, while the ellipticity signal amplitude simply decays. This turns out to be a direct consequence of the

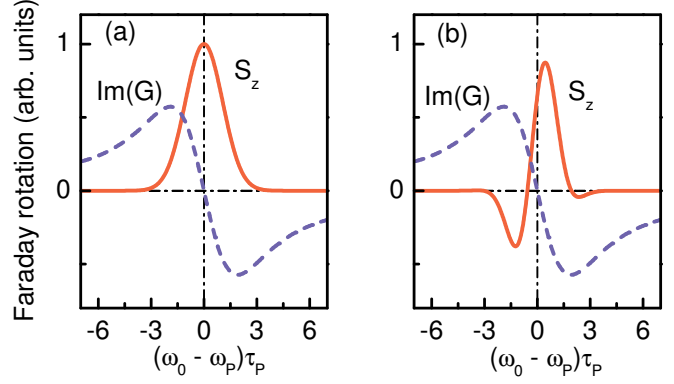


Figure 6: (Color online) Schematic illustration of Faraday rotation signal formation for degenerate pump-probe conditions, $\omega_{pr} = \omega_P$. Panel (a) corresponds to zero pump-probe delay, panel (b) to a pump-probe delay $t > 0$. Red curve shows initial spin distribution generated by the pump pulse, blue dashed curve shows the spectral sensitivity of the FR signal $\text{Im} G(\omega_0 - \omega_{pr})$.

correlation between Larmor frequency Ω_L and optical frequency.

At $t = 0$ the spin distribution is symmetric and gives zero FR signal since it is convoluted with the odd function, $\text{Im} G(\Lambda)$, as shown in Fig. 6(a). A non-zero Faraday signal can appear only due to some asymmetry. As time goes by, the electron spin distribution becomes asymmetric since spins in QDs with larger trion resonance frequencies ω_0 precess slower than the spins of QDs with smaller resonance frequencies because corresponding electron g factors are different, see Eq. (2). As a result, the distribution of electron spins as a function of resonance frequency is no longer symmetric with respect to the probe frequency ω_{pr} , see Fig. 6(b). Such an imbalance results in the appearance of non-zero Faraday rotation signal at $t > 0$. At relatively large delays the spin dephasing caused by the nuclear spin fluctuations and the spread of g -factors comes into play and the Faraday rotation signal amplitude decreases. The detuning between the pump and probe pulses results in the asymmetry of the spin distribution with respect to ω_{pr} even at $t = 0$. Hence, ordinary, decaying with time component of FR signal appears and growing with time component becomes less pronounced in line with experimental observations, Fig. 4(b).

For ellipticity, the spectral function $\text{Re} G(\Lambda)$ is even and is sensitive to the average spin z component which oscillates in time and decays due to the spread of Larmor frequencies.

The outlined model also explains qualitatively the difference between the FR and the ellipticity signals at negative pump-probe delays, $t < 0$, and the increase of the FR with increase of pump-probe time separation in this delay range. The signal at $t < 0$ appears because the sample is subject to a train of pump pulses. If the single electron spin relaxation time τ_s is much longer than the pulse repetition period, which is the case in our experiments,^{6,7} each electron preserves its spin coherence up to the moment of the next pump pulse arrival. As a result, spin precession mode-locking occurs: for electrons

with Larmor spin precession periods being commensurable with the pump repetition period the spin is accumulated as the pump pulses arrive in phase with the spin precession. Hence, the steady state distribution of precessing spins, $S_z^+(\omega_0, \omega_P)$, has sharp maxima for those QDs where $\Omega_L(\omega_0)T_R = 2\pi N$, N being an integer.^{4,6} If only these mode-locked spins are taken into account, the precession frequencies are commensurable with the repetition period and the signals are even functions of the pump-probe delay, t . The presence of other spin precession frequencies results in additional contributions to the spin signals at positive delays, $t > 0$, which dephases towards the moment of the next pump pulse arrival.

It is possible to obtain an analytical result for the ellipticity and the FR signals for a Gaussian distribution of the quantum dot resonant frequencies $p(\omega_0)$. In this case, the FR signal behavior depends on the spectral position of the pump pulse with respect to the maximum of the QD trion resonance frequency distribution. Indeed, for the absolutely symmetric situation at $t = 0$ the FR signal is zero. A shift of $\hbar\omega_P$ from the maximum results in an asymmetry of the photoexcited QD distribution, and, correspondingly, in a shift of the maximum of ellipticity and the zero of FR away from zero detuning.⁴ Such an asymmetry can be caused also by the transition energy variation of the trion oscillator strength in the QDs ensemble. The asymmetry discussed above does not require the inclusion of nuclear spin effects to describe the shifts of ellipticity and Faraday rotation signals from zero detuning, as was suggested in Ref. 12.

Now we turn to the spin precession frequencies. In our simplified model one can see that the effective spin precession frequency $\tilde{\Omega}_0$ in Eqs. (7a) and (7b) depends both on the spectral positions of the pump and the probe. It corresponds to the averaged optical frequency between pump and probe. Hence, the observed electron g factor which is evaluated from the experimental signals measured for non-degenerate conditions as function of the pump-probe detuning is approximately given by

$$|g_e(\Delta)| = a\hbar\omega_P + c - \frac{a}{2}\Delta, \quad (8)$$

i.e. its slope is twice smaller as compared to the slope of the $|g(\omega_0)|$ dependence, Eq. (2). This is because the observed g factor is an average of that at the pump and the probe frequencies. These functions are shown in Fig. 5 by the dashed [Eq. (8)] and dash-dotted [Eq. (2)] lines with constants $a \approx -0.004 \text{ meV}^{-1}$ and $|g_e(\omega_P)| \approx 0.55$. The spectral dependence of the g factor extracted from the ellipticity signal is well described within this simplified model, see Fig. 5(a).

The simplified model, however, does not describe well the g factor data obtained from the FR signal. It is seen in Fig. 5(b) that the experimental data have much weaker spectral dependence than the theoretical predictions. This discrepancy results from the fact that, for $\Lambda\tau_p \gtrsim 1$ the detuning dependence of $\text{Im} G(\Lambda)$ used in theory is much stronger than that in experiment. In fact, for weakly decaying $\text{Im} G(\Lambda)$ and relatively large detuning the convolution determining the Faraday rotation, Eq. (3), is controlled by the trion resonance frequencies corresponding to the maximum of $S_z^+(\omega_0, \omega_P)$,

i.e. the spin precession frequency is approximately given by $g(\omega_P)\mu_B B/\hbar$. Below, these findings are confirmed by numerical modeling.

C. Numerical modeling

The simple model discussed in Sec. IV B qualitatively describes the main features of the experiments. To perform a quantitative analysis and to eliminate the discrepancies between the FR spectral dependencies and the simple model we did numerical calculations in the frame of the model proposed in Ref. 4. The FR and ellipticity signals were calculated from Eq. (3), with the spectral function $G(\Lambda)$ corresponding to the Rosen&Zener laser pulse of proper duration, see Eq. (61) in Ref. 4. We also took realistic distributions of the electron g factors and optical frequencies: the constants a and c in Eq. (2) were extracted from the spectral dependence of the g factor in Fig. 5(a), see also Eq. (8), so that the g factor spread within the pulse spectral width was estimated to be $\Delta g = 0.002$. By comparing this value with the g factor spread extracted from the spin beats decay $\Delta g = 0.005$ we determine the additional fluctuations of the g factor, and, correspondingly, of the electron spin precession frequency $\Delta\Omega$, in Eq. (5) caused, e.g., by the nuclear spin fluctuations.²⁰

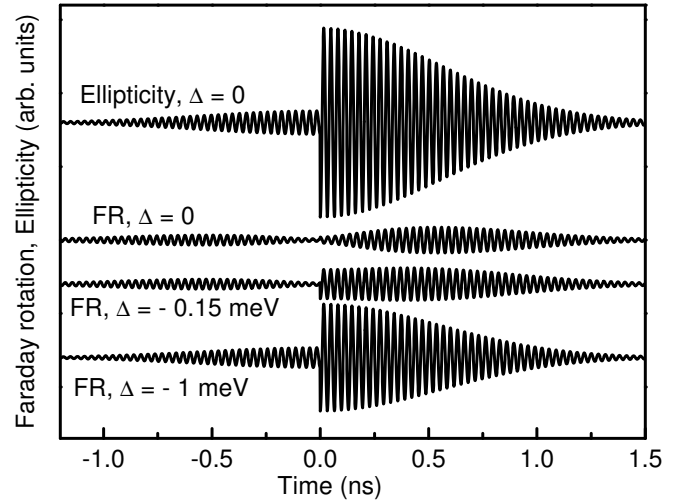


Figure 7: Modeled time-resolved Faraday rotation and ellipticity signals. The two upper dependencies show ellipticity and Faraday rotation signals for degenerate pump and probe, the two bottom dependencies show the Faraday rotation signal for detuned probe. Calculation parameters: $a = -0.004 \text{ meV}^{-1}$, $c = 6.142$, $\Delta g = 0.005$, $\Theta = 0.2$, $T_R = 13.2 \text{ ns}$, $\tau_p = 3 \text{ ps}$.

Figure 7 shows calculated ellipticity and Faraday rotation signals for degenerate and nondegenerate pump-probe arrangements. The modeled signals are very similar to the experimental ones shown in Fig. 1(a), see also Fig. 3. The parameters of calculation were chosen in a such a way that the calculated signals and measured ones are as similar as possible. The effective pulse area Θ , which determines the electron spin change by the pump

pulse,⁴ was estimated from the experimental spin signal amplitudes before and after the pump pulse arrival to be $\Theta \approx 0.2$. The duration of the Rosen&Zener pulse used in the calculations was chosen to be $\tau_p = 3$ ps in order to reproduce properly the temporal shape of experimental pulse and widths of the signal amplitudes spectral dependencies.

A fitting procedure similar to the one applied to the experimental data was used also for extraction of the amplitudes of the calculated ellipticity and Faraday rotation signals. Solid and dashed lines in Fig. 4 show the calculated spectral dependencies of these amplitudes, which almost perfectly match the experimental points. The discrepancy between the calculated and the experimental α_{neg} for the ellipticity signal in Fig. 4(a) may result from nuclear effects.⁷

The solid and dashed curves in Fig. 5 give the calculated spectral dependencies of the electron g factor extracted from the ellipticity and FR signals. The complicated non-monotonous dependence of the g factor in the FR signal for moderate detuning results from the complex shape of the spectral function for the FR signal. The calculation shows, that the spin beats occur at multiple frequencies corresponding, e.g., to the maxima and minima of the Faraday rotation spectral function and to the spin distribution maxima. As a result, fitting of this behavior by the simplified Eq. (1) gives an averaged g factor which oscillates with the detuning in the ranges where the spectral function and the pump-induced spin distribution strongly overlap. In agreement with the experiment, the spectral dependence of the g factor in the ellipticity signal is stronger than that in FR. Good agreement between the experiment and theory is achieved.

V. CONCLUSIONS

We have studied in detail the Faraday rotation and ellipticity signals in singly-charged (In,Ga)As/GaAs quantum dot ensembles. Not only the amplitudes, but also the temporal behavior of the ellipticity and Faraday rotation signals are qualitatively different. For degenerate pump and probe pulses the Faraday rotation signal first grows as a function of time separation between the two pulses and then decays, while the ellipticity starts from its maximum value for zero time separation and then de-

cays. We have demonstrated also, that the spin beat frequencies measured as a function of the probe spectral position are quite different for Faraday rotation and ellipticity. In the latter case, the spin precession frequency changes linearly with pump-probe detuning, while in the former case the spin precession frequency does not change much with detuning.

The experimental findings are well explained within the developed theoretical formalism, which takes into account the microscopic processes responsible for pump-probe signal formation and the inhomogeneity of the quantum dot ensemble. For degenerate pump and probe pulses, the Faraday rotation signal is sensitive to the asymmetry of the electron spin distribution. Such an asymmetry appears with time due to the correlation between the electron g factor and the trion resonance frequency, ω_0 . On the other hand, the ellipticity signal measures the averaged electron spin and is therefore much less sensitive to the distribution asymmetry.

The increase of the Faraday rotation signal with pump-probe time separation results from the dependence of the electron g factor on the effective band gap. Hence, a similar temporal behavior can be observed not only for the long-lived resident electron signal, but also for the electron spin beats in empty quantum dots. In the latter case, however, the exchange interaction between electron and hole in the exciton can make a considerable contribution to the spin beat frequency, masking the spectral dependence of the g factor.

We have shown both experimentally and theoretically that the Faraday rotation and ellipticity effects probe different parts of the inhomogeneous quantum dot ensemble. Quantitative agreement between theory and experiment, including comparison of the spectral dependencies of signal amplitudes and spin beats frequencies, has been achieved.

Acknowledgments

We are grateful to Al.L. Efros and E.L. Ivchenko for valuable discussions. This work was supported by the BMBF project nanoquit, the Deutsche Forschungsgemeinschaft and Russian Foundation for Basic Research. M.M.G. is thankful to the “Dynasty” Foundation—ICFPM and President grant for young scientists.

¹ *Spin Physics in Semiconductors*, Ed. M. I. Dyakonov (Springer-Verlag, Berlin, 2008).

² *Semiconductor Spintronics and Quantum Computation*, Eds. D. D. Awschalom, D. Loss, and N. Samarth (Springer-Verlag, Berlin, 2002).

³ B. Beschoten, in *Lecture Manuscripts of the 36th Spring School of the Institute of Solid State Research “Magnetism Goes Nano”*, ed. by S. Bluegel, Th. Brueckel, and C. M. Schneider, Reihe Matter and Materials (Forschungszentrum Juelich GmbH, 2005), Vol. 26, p. E7.1.

⁴ I. A. Yugova, M. M. Glazov, E. L. Ivchenko, and Al. L. Efros, *Phys. Rev. B* **80**, 104436 (2009).

⁵ A. Greilich, R. Oulton, E. A. Zhukov, I. A. Yugova, D.

R. Yakovlev, M. Bayer, A. Shabaev, Al. L. Efros, I. A. Merkulov, V. Stavarache, D. Reuter, and A. Wieck, *Phys. Rev. Lett.* **96**, 227401 (2006).

⁶ A. Greilich, D. R. Yakovlev, A. Shabaev, Al. L. Efros, I. A. Yugova, R. Oulton, I. V. Stavarache, D. Reuter, A. Wieck, and M. Bayer, *Science* **313**, 341 (2006).

⁷ A. Greilich, A. Shabaev, D. R. Yakovlev, Al. L. Efros, I. A. Yugova, D. Reuter, A. D. Wieck, and M. Bayer, *Science* **317**, 1896 (2007).

⁸ I. A. Yugova, A. Greilich, E. A. Zhukov, D. R. Yakovlev, M. Bayer, D. Reuter, and A. D. Wieck, *Phys. Rev. B* **75**, 195325 (2007).

⁹ The maximum of ellipticity signal and the zero of FR sig-

nal (also the maxima of amplitudes β of the FR signal) are slightly shifted from zero detuning between pump and probe. We discuss possible reasons for this shift below, in Sec. IV.

- ¹⁰ L. V. Fokina, I. A. Yugova, D. R. Yakovlev, M. M. Glazov, I. A. Akimov, A. Greilich, D. Reuter, A. D. Wieck, and M. Bayer, Phys. Rev. B **81**, 195304 (2010).
- ¹¹ M. H. Mikkelsen, J. Berezovsky, N. G. Stoltz, L. A. Coldren, and D. D. Awschalom, Nature Physics **3**, 770 (2007).
- ¹² S. G. Carter, A. Shabaev, Sophia E. Economou, T. A. Kennedy, A. S. Bracker, and T. L. Reinecke, Phys. Rev. Lett. **102**, 167403 (2009).
- ¹³ E. L. Ivchenko, *Optical Spectroscopy of Semiconductor Nanostructures* (Alpha Science, Harrow UK, 2005).
- ¹⁴ I. A. Yugova, A. Greilich, D. R. Yakovlev, A. A. Kiselev, M. Bayer, V. V. Petrov, Yu. K. Dolgikh, D. Reuter, and A. D. Wieck, Phys. Rev. B **75**, 245302 (2007).
- ¹⁵ E. A. Zhukov, D. R. Yakovlev, M. Bayer, M. M. Glazov, E.

L. Ivchenko, G. Karczewski, T. Wojtowicz, and J. Kossut, Phys. Rev. B **76**, 205310 (2007).

- ¹⁶ Sophia E. Economou, L. J. Sham, Yanwen Wu, and D. G. Steel, Phys. Rev. B **74**, 205415 (2006).
- ¹⁷ E. A. Zhukov, D. R. Yakovlev, M. M. Glazov, L. Fokina, G. Karczewski, T. Wojtowicz, J. Kossut, and M. Bayer, Phys. Rev. B **81**, 235320 (2010).
- ¹⁸ Making use of the explicit expressions in Ref. 4 one can show that $\text{Im } G(\Lambda) \propto (\Lambda \tau_p)^{-1}$.
- ¹⁹ It is also possible to obtain analytical expression for exponential pump and probe pulses with envelopes $\propto \exp(-|t|/\tau_p)$, but the resulting expressions are cumbersome and do not result in qualitatively new physical effects.
- ²⁰ A. Greilich, S. Spatzek, I. A. Yugova, I. A. Akimov, D. R. Yakovlev, Al. L. Efros, D. Reuter, A. D. Wieck, and M. Bayer, Phys. Rev. B **79**, 201305 (R) (2009).